

Peak Effect in Superconductors: Absence of Phase Transition and Possibility of Jamming in Vortex Matter*

Mahesh Chandran[†]

(Dated: February 8, 2020)

The magnetic field B dependence of the critical current I_c for the vortex phase of a disordered superconductor is studied numerically at zero temperature. The $I_c(B)$ increases rapidly near the upper critical field B_{c2} similar to the peak effect (PE) phenomenon observed in many superconductors. The real space configuration across the PE changes continuously from a partially ordered domain (polycrystalline) state into an amorphous state. The topological defect density $n_d(B) \sim e^{\alpha B^k}$ with $k > 1$ for $B \geq 0.4B_{c2}$. There is no evidence of a phase transition in the vicinity of the PE suggesting that an order-disorder transition is not essential for the occurrence of the PE phenomenon. An alternative view is presented wherein the vortex system with high dislocation density undergoes jamming at the onset of the PE.

PACS numbers:

I. INTRODUCTION

The critical current density J_c for a type-II superconductor decreases monotonically as a function of the magnetic field B or the temperature T over most part of the B - T phase diagram. But quite often, a peak in the $J_c(B)$ (or $J_c(T)$) is observed close to the upper critical field $B_{c2}(T)$ (or critical temperature $T_c(B)$). This phenomenon is known as the peak effect (PE) and was first studied in 1961. Extensive work since then have shown that PE exist in wide class of materials which includes low- T_c (Nb and its alloys[1], V₃Si[2], NbSe₂[3]), high- T_c (YBa₂Cu₃O₇[4]), heavy fermion (UPt₃[5], UPd₂Al₃[6]), and other exotic (Sr₂RuO₄[7]) superconductors, including the recently discovered compound MgB₂[8]. Apart from single crystals, the phenomenon have been observed in polycrystalline and thin amorphous films[9]. The PE is found to be more pronounced in the weak pinning limit and progressively diminishes with increasing pinning strength[10, 11]. An important characteristic of the PE phenomenon is the strong memory and history dependence of the various properties, and have been observed in static and dynamic experiments[12, 13, 14, 15, 16, 17].

The explanation for the PE is based on the softening of the vortex lattice with increasing B , first suggested by Pippard[18]. If the vortex lattice rigidity falls more rapidly than the elementary vortex pinning strength f_p as $B \rightarrow B_{c2}$, the softening would allow vortices to conform to the random pinning potential better compared to a stiff vortex lattice. This idea was further developed and quantified in the collective pinning theory by Larkin

and Ovchinnikov[19] (LO). In the LO theory, the vortex lattice is broken into coherently pinned regions of volume $V_c = R_c^2 L_c$ within which the pinning forces act randomly. R_c and L_c are the transverse and the longitudinal correlation lengths, respectively, and are related to the tilt modulus C_{44} and the shear modulus C_{66} of the vortex lattice. The balancing of elastic energy and the pinning energy within V_c gives the critical current density $J_c \propto f_p(n_p/V_c)^{1/2}$. LO suggested that in 3D the spatial dispersion of C_{44} can lead to an exponential decrease in V_c near B_{c2} giving rise to the PE phenomenon. The PE is not expected in the 2D since the only relevant elastic modulus C_{66} is weakly dispersive.

Experimentally, the PE have been observed in thin amorphous films (samples with thickness $d < L_c$). This was interpreted within the collective pinning theory as due to dimensional crossover from 2D to 3D in the pinning characteristic[20]. Recently, the PE have been observed in ultra thin Bi films of $d = 26\text{ \AA}$ [21] which is difficult to account for within the dimensional crossover scenario. Moreover, neutron scattering experiment on Nb crystal shows that L_c actually increases with B , and the decrease in L_c in the PE region is not appreciable[22]. Also, the LO theory cannot account for the PE in $J_c(T)$ [23].

In the LO picture, the pinning energy overcomes the elastic energy beyond R_c , and hence, the long range order is not expected to survive in the vortex lattice. In high- T_c superconductors, topologically ordered vortex lattice on a length scale $r \gg R_c$ was observed[24, 25]. Detailed calculations showed that in the presence of weak point impurities a quasi-long range ordered vortex lattice survives in 3D with $C(r) \sim r^{-\eta}$, where η is a non-universal exponent[26, 27]. Such a phase has been termed as the Bragg glass (BG). The BG undergoes a first-order melting transition into a vortex liquid (VL) phase on increasing T . Also, the BG undergoes a weak first-order transition into the vortex glass (VG) phase on increasing B [28]. In the VG phase, the plastic deformation caused by the topological defects leads to strong pinning, and

*This work was carried out during the authors' stay in the Department of Physics, University of California, Davis, 95616.

[†]Present Affiliation: Materials Research Laboratory, John F Welch Technology Centre, GE India Technology Centre, Phase 2, Hoodi Village, Whitefield Road, Bangalore, 560066; Email address: mahesh.chandran@ge.com

hence higher J_c compared to the BG phase. The PE have thus been interpreted as a consequence of an order-disorder transition[29, 30]. Furthermore, the origin of anomalous dynamics near the PE is attributed to the coexistence of BG and VG phases in the vicinity of the transition[31, 32].

Interpretation of the PE phenomenon as an order-disorder transition has limitations. Firstly, the BG phase is not expected in 2D[33], and hence order-disorder transition cannot account for the PE in amorphous films. Secondly, the BG phase have been shown theoretically to exist in the presence of weak point impurities. It is not clear if the BG would survive in polycrystalline samples in which the PE has been well documented. Recent Bitter decoration of NbSe_2 across the PE shows no distinct ordered and disordered phases[34]. Also, the width of the field range in which the ordered and the disordered phases coexist have been shown to scale with the sample size, which is an evidence against the phase transition interpretation of the PE[35].

Attempts have been made to understand the PE phenomenon using numerical simulation. Cha and Fertig[36] used an attractive term in the inter-vortex potential to tune the C_{66} in 2D. A small peak in the total depinning force was observed which was associated with the transition from the elastic to plastic depinning. But as emphasized in Ref.[37], the peak in total depinning force as a function of C_{66} does not imply a peak in $J_c(B)$. Later simulation in 3D showed an insignificantly small peak near the BG to VG transition[38]. The PE was also studied in a model of layered superconductors where the peak in J_c was induced through the decoupling transition[39].

In this paper, the behaviour of the critical current $I_c(B)$ for a 2D disordered vortex matter is studied using numerical simulation. The effect of finite vortex core is included in the inter-vortex interaction and is shown to be essential for the realistic description of the system close to B_{c2} . The $I_c(B)$ decreases monotonically in the intermediate field range and rises rapidly close to B_{c2} similar to the PE phenomenon observed in real systems. The vortex configuration shows no order-disorder transition but a continuous transformation from a polycrystalline domain state below the PE to a liquid-like amorphous state in the PE region. An alternative scenario for the PE is discussed where the vortex system undergoes jamming due to increased dislocation density. An empirical relation between the $I_c(B)$ and the real space defect density is also obtained from the simulation which captures the essential physics governing the behaviour of $I_c(B)$ for a disordered vortex matter.

The paper is organized as follows: in section 2, the simulation details are presented, followed by results in section 3. The results are discussed in Section 4, and the conclusions are summarized in Section 5.

II. SIMULATION METHOD

Consider a 2D cross-section of a bulk type-II superconductor perpendicular to the magnetic field $\mathbf{B} = B\hat{\mathbf{z}}$. We model the vortices as classical particles interacting via two-body potential, and governed by an overdamped equation of motion

$$\eta \frac{d\mathbf{r}_i}{dt} = - \sum_{j \neq i} \nabla U_C^v(\mathbf{r}_i - \mathbf{r}_j) - \sum_k \nabla U^p(\mathbf{r}_i - \mathbf{R}_k) + \mathbf{F}_{ext}, \quad (1)$$

where η is the flux-flow viscosity. The first term on the left hand side represents the inter-vortex interaction, and the second term is the attractive interaction between the vortex and the quenched impurities. \mathbf{F}_{ext} is the Lorentz force on the vortex due to an applied current. Each of the three terms are further discussed in detail below.

The inter-vortex potential $U_C^v(r) = \frac{\phi_0^2}{8\pi^2\lambda^2} K_0(\tilde{r}/\lambda)$, where K_0 is the modified Bessel function, and $\tilde{r} = (r^2 + 2\xi^2)^{1/2}$. ϕ_0 is the flux quantum, and λ and ξ are the penetration depth and the coherence length of the superconductor respectively. This form of the interaction was derived by Clem from the Ginzburg-Landau (GL) equation using variational method[40, 41]. Conventionally, the vortex dynamics have been studied using the potential $U_L^v(r) = \frac{\phi_0^2}{8\pi^2\lambda^2} K_0(r/\lambda)$ which is derived from the London's equation. For small r , the $K_0(r) \propto -\ln(r)$, leading to an unphysical singularity in $U_L^v(r)$ as $r \rightarrow 0$. The potential $U_L^v(r)$ is thus inadequate for describing correctly the vortex core region which limits its applicability to small B . On the other hand, Clem's potential $U_C^v(r)$ is well behaved as $r \rightarrow 0$ and gives realistic form of the magnetic flux density $\mathbf{B}(r)$ and the supercurrent density $\mathbf{J}(r)$ near the vortex core region. The correct description of the vortex core region is essential to extend the simulation to high magnetic fields where the cores of the neighboring vortices tend to overlap.

An important consequence of using Clem's potential is that the vortices are not point particles but have a finite radius ξ . This is an improvement over the previous simulations which treated vortices as point particles interacting via London's potential $U_L^v(r)$. Note that the London's model of vortices interacting via two-body potential is strictly valid for $B < 0.25B_{c2}$ [41]. Even though Clem's potential overcomes some of the limitations of the London's potential at high fields, it still provides only a qualitative behaviour of the vortex system. A more realistic approach for understanding the vortex dynamics close to B_{c2} is through the time dependent GL theory (TDGL). Unfortunately, the computation cost for TDGL is prohibitive even for a small sample size[42] which restricts its utility.

The second term in Eq.(1) is the attractive force between the vortex and the quenched impurities which act as pinning centers. The force is derived from the parabolic potential, $U^p(r) = U_0(\frac{r^2}{r_p^2} - 1)$ for $r < r_p$, and 0 otherwise. The impurities are randomly placed at positions \mathbf{R}_k in the simulation box. The third term

is the Lorentz force $\mathbf{F}_{ext} = \frac{1}{c}\mathbf{J} \times \phi_0\hat{\mathbf{z}}$ where \mathbf{J} is the current density. A uniform current density along the y -direction is assumed such that all vortices experience the same force F_{ext}^x along the x -direction. For the simulation purpose, the length is defined in units of $\lambda(B=0) = \lambda_0$. The current density J and the velocity of the vortex v_x are in the units of cf_0/ϕ_0 and f_0/η , respectively, where $f_0 = \frac{\phi_0^2}{8\pi^2\lambda_0^3}$. From the relation $\mathbf{E} = \mathbf{v} \times \mathbf{B}$, the $v_x \propto E_y \propto V$ where V is the voltage generated in the direction of the current $I \propto J_y \equiv F_{ext}^x$. Hence, the $v_x(F_{ext}^x)$ behavior represents the $V(I)$ characteristic (or equivalently $E(J)$ curve) for a superconductor.

The dimensionless magnetic field is defined as $b = B/B_{c2}$, where the upper critical field $B_{c2} = \frac{\phi_0}{2\pi\xi_0^2}$ and $\xi_0 = \xi(B=0)$. The b is calculated from the lattice constant $\frac{a_0}{\lambda_0} = (\frac{4\pi}{\sqrt{3}})^{\frac{1}{2}}(\frac{1}{\kappa^2 b})^{\frac{1}{2}}$. The GL parameter $\kappa = \frac{\lambda}{\xi}$ is an input to the simulation. In the GL theory, the length scale λ and ξ increases with b and diverges as $b \rightarrow 1$. The renormalization of λ and ξ with increasing b is included in the simulation through the relation $\lambda(b) = f(b)\lambda_0$ and $\xi(b) = f(b)\xi_0$, where $f(b) = 1/\sqrt{1-b^2}$. This form of $f(b)$ is similar to the T -dependence of ξ in the GL theory[43] with T/T_c replaced by $(B/B_{c2})^2$, and have been used previously in Ref.[44]. The same form of $f(b)$ is chosen for λ and ξ in order to keep κ independent of B .

The simulation was carried out by numerically integrating the equation of motion using the fourth order predictor-corrector scheme. Parallel algorithms were implemented details of which can be found in Ref.[45]. A perfect vortex lattice driven by a large current $I \gg I_c$ was used as the starting condition for the simulation. The I is then reduced to 0 in small steps and the average voltage V was calculated in the steady state at each step to obtain the $V(I)$ curve. In the dimensionless units defined above, the $V = I$ in the asymptotic limit $I \rightarrow \infty$. The I_c is defined as the current at which the $V \lesssim 10^{-5}$ [46]. The procedure used for obtaining the $V(I)$ curve was motivated by experiments where a stable vortex configuration is observed if the system is brought to rest after driven with $I \gg I_c$ [47]. Also, the $I_c(b)$ from such a method shows the largest peak compared to that obtained from the field-cooling experiments.

The real space configuration of vortices was characterized by locating the topological defects in the system using Delaunay triangulation. For the triangular vortex lattice, a topological defect is a vortex with coordination number other than 6. The defect density n_d/λ_0^2 is defined as the number of defects per unit area of the simulation box. Most of the defects form dislocations which are bound pair of disclinations (vortices with coordination 5 and 7). The fraction of free disclination is small over a wide range of fields, and hence $n_d \approx 2n_{disl}$ where n_{disl} is the dislocation density. Along with the $V(I)$ curve, the behaviour of $n_d(I)$ was also determined for each value of b . The n_d discussed below represents the defect density at $I = 0$, unless specified otherwise.

The parameters used in the simulation are $\kappa = 10$ and $\lambda(B=0) = 1000\text{\AA}$. These values are typical of low- T_c superconductors, particularly NbSe₂. The periodic boundary conditions were imposed in both directions. The magnetic field b was varied by changing the size of the simulation box, keeping the number of vortices N_v fixed (for smaller system size, N_v is also allowed to vary between 800-1200). The results presented below are for $N_v = 4096$. The prefactor U_0 of the pinning potential $U^p(r)$ is distributed randomly between $\Delta \pm 0.01$ where $\Delta = \langle U_0 \rangle$. The simulation is restricted to point impurities with the range of the pinning potential $r_p = \xi_0$. The pin density $n_p = 2.315/\lambda_0^2$. The dilute limit of n_p is chosen keeping in mind that the PE is observed close to B_{c2} where the concentration of effective pinning centre is expected to be very small.

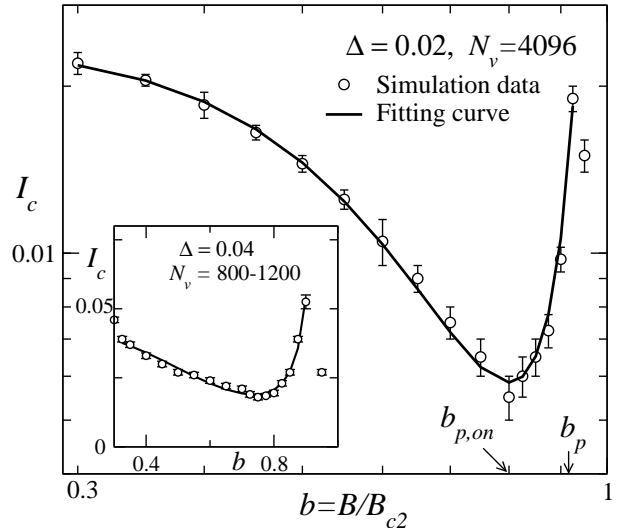


FIG. 1: The critical current $I_c(b)$ for $\Delta = 0.02$ and $N_v = 4096$. The $I_c(b)$ for $\Delta = 0.04$ is shown in the inset. For this plot, the N_v was also varied between 800 and 1200 along with the simulation box size. The thick line represents the fit to the simulation data (shown by open symbols).

III. RESULTS

A. Critical current $I_c(b)$

Figure 1 shows the $I_c(b)$ for $\Delta = 0.02$. For $b < b_{p,on} = 0.8$, the I_c decreases monotonically. At $b_{p,on}$, the $I_c(b)$ turns around and rises rapidly till $b = 0.925$. The rapid increases in I_c above $b_{p,on}$ signals the appearance of the PE. The inset shows the PE for $\Delta = 0.04$ for which a smaller system size was used. The $b_{p,on}$ decreases from a value of 0.9 for $\Delta = 0.01$ to 0.75 for $\Delta = 0.04$. The proximity of the PE to the upper critical field B_{c2} is in good agreement with the experiments.

For $b > b_p = 0.925$, the I_c decreases. For $b \geq 0.95$

two vortices occasionally come together to form an effective vortex with charge $2\phi_0$. Overlapping of the two vortex cores is strongly influenced by the impurities. This was confirmed by simulating without the pinning centres where no overlapping of the vortices was found up to $b = 0.98$. The effective interaction between a $2\phi_0$ vortex and the ϕ_0 vortex is greater than the interaction between ϕ_0 vortices. This enhances the local rigidity of the vortex system, and possibly decrease the I_c . It is worth mentioning that a short range attractive interaction exist between the vortex cores[41] which is not included in the simulation. The important point is that the overlapping of vortex cores is observed for $b \geq 0.95$, and hence does not influence the increasing branch of the PE. It is possible that the $I_c(b)$ above b_p is influenced by the overlapping of vortices, a issue which can be addressed only by solving TDGL equations in the presence of impurities.

Attempts were made to fit the $I_c(b)$ data to a single function across the PE. A reasonably good fit was obtained using the expression

$$I_c(b) = I_{c0} \exp(-\beta b^k) \frac{1}{(1-b^2)^4}, \quad (2)$$

with $k \approx 2.6$ and $\beta \approx 9.75$ for $\Delta = 0.02$. For $\Delta = 0.04$, $k \approx 2.4$ and $\beta \approx 8.3$. The above function was motivated by the behaviour of the $n_d(b)$ which follows the same exponential form, whereas the dependence on $\frac{1}{(1-b^2)}$ reflects the behaviour of λ and ξ as $b \rightarrow 1$. The renormalization of the length scales λ and ξ leads to weak inter-vortex interaction, and explains why the PE in real system occurs close to the $B_{c2}(T)$ line. As shown below, the bare length scale λ_0 and ξ_0 leads to a stiff vortex lattice for $b > 0.6$ and consequently the PE is absent.

B. $V(I)$ characteristics across the Peak Effect

Figure 2 shows the $V(I)$ curves across the PE. The curves for high- b crosses the curves for low- b in the sub-ohmic region. The crossing can be understood from the dynamics close to I_c . For $I \gtrsim I_c$, the dynamics is heterogeneous with few vortices moving in channels in a background of defective vortex configuration[48, 49, 50]. The width of the channels $\sim a_0$ and display large transverse wandering relative to the direction of the Lorentz force. Since not all vortices are active, the voltage response is sub-ohmic. The number of active channels increases with I , and for $I = I_p$ all vortices move in channels which are ordered transverse to the flow direction. The time-averaged defect density shows an abrupt drop at I_p , and represents annealing of the plastic deformation (some dislocations with Burger vector parallel to the Lorentz force can exist for $I > I_p$). For $I > I_p$, the response is ohmic and the resistance approaches the free flux-flow value. The sub-ohmic response window $\delta I_{dis} = I_p - I_c$ thus quantify the extent of plastic deformation of the vortex system. As shown in Ref.[51], $\delta I_{dis}(b)$ increases rapidly

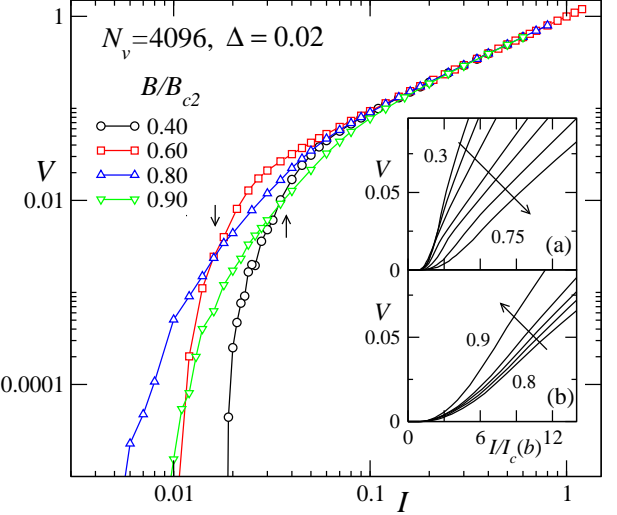


FIG. 2: The $V(I)$ curve across the PE. Arrows point to the crossing of $V(I)$ curves. Inset: the $V(I/I_c(b))$ curves for (a) $b < b_{p,on}$, and for (b) $b \geq b_{p,on}$. The arrows represent the direction of increasing b . The magnetic fields in (a) are 0.3, 0.4, 0.5, 0.6, 0.65, 0.7 and 0.75. In (b), the b increases from 0.8 to 0.9 in steps of 0.025.

in the PE region implying that larger currents are required to anneal the defects. This is reflected in the slow growth of $V(I)$ curve for high fields, which consequently cross the curves for low fields as shown in Fig. 2.

The inset in Fig. 2 shows the change in $V(I)$ characteristics as b is varied across the PE. For each curve, the I is scaled by the respective $I_c(b)$. Far below the PE, the curves are convex for $I \gtrsim I_c$. As b approaches $b_{p,on}$, the curvature changes to concave. The concave part of the $V(I)$ curve indicates a slow growth of the response due to increased plasticity of the system. Interestingly, for $I/I_c(b) > 1$, the $V(b)$ reflects the non-monotonic behaviour of $I_c(b)$. Thus, the PE is characterized by static as well as dynamic changes in the system, and agrees with the conclusion from the experiments[52].

C. Real space configuration

The simulation allows the changes in the real space configuration to be characterized precisely, thus allowing theories based on configurational changes to be tested. Fig. 3 shows the real space images at $I = 0$ in a region of the simulation box as b is changed across $b_{p,on}$. The defects are marked by filled circles. A topologically ordered vortex lattice is not observed for any value of b consistent with the theory for 2D system[26]. But partial order can still be seen in large domains for b between 0.3 – 0.6. The dislocations are arranged in string-like structures and forms the grain boundary (domain walls). There are no free dislocations inside the domain, and free disclinations are absent below $b_{p,on}$. The configuration in

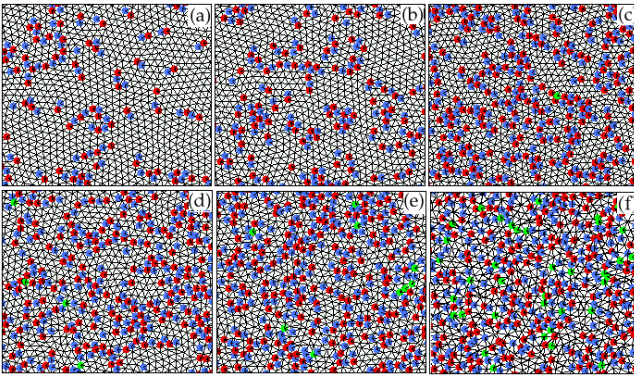


FIG. 3: The Delaunay triangulation of the real space configuration across $b_{p, on}$. The $b=0.70$ (a), 0.75 (b), 0.80 (c), 0.85 (d), 0.875 (e), and 0.90 (f). The red and the blue dots represents vortices with 7 and 5 neighbors, respectively. The vortices with 4 and 8 neighbors are denoted by the green dot. The pinning strength $\Delta = 0.02$ and $N_v = 4096$. Only a small region of the simulation box is shown for clarity.

the intermediate fields is reminiscent of a polycrystalline solid. With increasing b , the domain size decreases but the increase in the defect density occurs *within* the grain boundaries. Some of the domains can also be seen for $b = 0.70$ and 0.75 . The average size of the domains decreases from $\approx 6a_0$ below the PE to $\approx 3a_0$ on the increasing branch of $I_c(b)$. At b_p , the configuration is amorphous (Fig. 3(d)) with defects forming a dense homogeneous network. It is not possible to isolate individual dislocations and the configuration is that of a frozen liquid[54].

The continuous transformation of a less disordered state below $b_{p, on}$ into an amorphous state at b_p precludes an order-disorder (or BG to VG) transition underlying the PE. The PE is thought to be due to such a phase transition in the vortex system[29]. The real space images shown in Fig. 3 is strikingly similar to the recent Bitter decoration of NbSe_2 in the PE region[34], which lends support to the idea that a phase transition is not necessary for the PE to occur. The amorphous state at b_p is also consistent with the neutron scattering experiment[22] and the STM imaging of the vortices[55] in the PE region.

D. Defect density $n_d(b)$

Figure 4(a) shows the defect fraction $f_d(b)$, defined as the ratio of number of defects to number of vortices, for $\Delta = 0.02$. As mentioned earlier, reducing I to zero from $I \gg I_c$ generates a configuration which is stable and does not show hysteresis[47]. The $f_d(I = 0)$ can thus be considered as the equilibrium defects which determines the behaviour of stable $I_c(b)$. The f_d is typically greater than 0.35 for $b < 0.1$. Similar value for f_d is reached at the onset of PE. The intermediate polycrystalline state

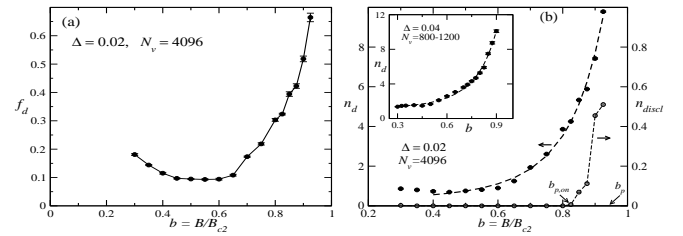


FIG. 4: (a) The defect fraction $f_d(b)$ at $I = 0$. (b) The defect density $n_d(b)$ at $I = 0$. The $n_{discl} = |n_{d,7} - n_{d,5}|$ is the approximate density of free disclinations, where $n_{d,7}$ and $n_{d,5}$ are the density of vortices with coordination number 7 and 5, respectively. Inset: the $n_d(b)$ plot for $\Delta = 0.04$. The thick dashed line is a fit to $n_d(b) = n_{d0} \exp(\alpha b^k)$.

is sandwiched between $0.3 \lesssim b \lesssim 0.7$, with f_d less than 0.2.

Interestingly, if the defect density $n_d(b)$ rather than $f_d(b)$ is plotted, a good fit can be obtained for $b \gtrsim 0.4$ using the expression

$$n_d(b) = n_{d0} \exp(\alpha b^k). \quad (3)$$

This is shown in Fig. 4(b) for $\Delta = 0.02$ and $\Delta = 0.04$ (inset). The exponent $k \approx 2.6$ and 2.4 for $\Delta = 0.02$ and 0.04 , respectively. Surprisingly, both $n_d(b)$ and $I_c(b)$ can be fit using the same value of k . This allows one to write

$$I_c(b) = \frac{I_{c1}}{[n_d(b)]^r} \frac{1}{(1 - b^2)^4}, \quad (4)$$

where $r \approx 2.5$ and 2.7 for $\Delta = 0.02$ and 0.04 , respectively. Figure 4(b) also shows the density of free disclinations which can be approximately defined as $n_{discl} = |n_{d,7} - n_{d,5}|$, where $n_{d,7}$ and $n_{d,5}$ are the density of vortices with coordination number 7 and 5, respectively. The n_{discl} is 0 for $b < b_{p, on}$, and rises rapidly in the PE region.

From the analysis of the $n_d(b)$ and the $I_c(b)$ data, it is possible to conclude that $I_c(b) \propto [n_d(b)]^{-r}$, where the effect of the pinning potential is implicit through the defect density $n_d(b)$ and the exponent r . This empirical relation between $n_d(b)$ and $I_c(b)$ captures the essential physics governing the behaviour of the critical current in a disordered vortex system with point impurities. Physically, the increase in n_d with b enables plastic shearing to be initiated at lower currents, which explains the monotonic decrease in I_c below the PE. But this also leads to a paradoxical situation: since the $n_d(b)$ continues to rise rapidly even in the PE region, the enhanced plasticity of the system should cause the I_c to decrease continuously till B_{c2} , contrary to the observation of PE above $b_{p, on}$. The problem is compounded further since the real space images do not suggest any noticeable configurational change across $b_{p, on}$ which can be associated with sudden increase in pinning due to quenched impurities.

The above paradox can be resolved by conjecturing that the vortex system undergoes jamming at the onset

of the PE due to increase in dislocation density. The jamming envisaged here is similar to the jamming in granular materials where the system develops a finite yield stress at a threshold packing fraction[56]. The jamming have been also studied in dislocation network formed in a plastically deformed material[57] which also shows complex spatio-temporal dynamics[58]. The jamming in the vortex system could occur due to disordered packing of vortices which imposes kinematic constraint for the motion of vortices. From Fig. 4(a), the defect fraction f_d becomes 0.30 at $b_{p, on}$, which could possibly be the threshold value for the jamming to occur in the vortex system. As mentioned earlier, the dynamics close to the I_c is governed by few active channels. The effect of disordered packing of vortices is to increase the effective energy barrier ΔE_T for the transverse mobility of the channel, thus requiring larger current to initiate channel dynamics. Future work should be able to obtain the B -dependence of ΔE_T , which could provide evidence for jamming in the PE region.

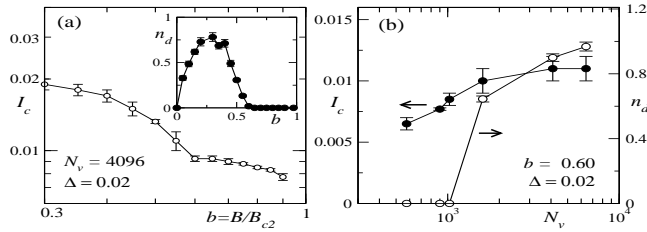


FIG. 5: (a) The $I_c(b)$ and $n_d(b)$ (inset) without the field dependence of the length scales λ and ξ . The $\Delta = 0.02$ and $N_v = 4096$. (b) The I_c and n_d as a function of N_v for $b = 0.6$ and $\Delta = 0.02$

E. Field independent λ and ξ

The $I_c(b)$ and the $n_d(b)$ obtained using $\lambda(b) = \lambda_0$ and $\xi(b) = \xi_0$ are shown in Fig. 5(a). The λ_0 and ξ_0 are the values at $B = 0$. For $b < 0.6$, the $I_c(b)$ does not show any appreciable deviation from that of Fig. 1. At $b \approx 0.6$, the defect density n_d becomes zero, and the system remains topologically ordered till B_{c2} . As a consequence, the PE is absent at high fields and is consistent with the idea that the PE cannot occur in rigid vortex lattice.

F. Finite size effect

The finite size effect on n_d and I_c was determined by increasing N_v for $b = 0.6$. The total number of defects shows a minimum around $b = 0.60$, or equivalently, the average size of the ordered region (domain) is maximum for this field. Hence, any relevant length scale determining the system behaviour would be largest for $b = 0.6$. Figure 5(b) shows I_c and n_d as a function of the system

size ($\propto N_v$). The maximum N_v which could be simulated was 6400. For $N_v \gtrsim 4000$, the I_c tends to become independent of the system size though n_d continues to increase, suggesting that the two quantities are determined by different length scales. The finite size calculation also shows that the system size used is sufficient to obtain macroscopic behaviour of the $I_c(b)$, and demonstrates the necessity of going to larger system size for doing realistic simulation of the vortex dynamics.

IV. DISCUSSIONS

The results presented above clearly demonstrates that a phase transition is not essential for the PE to occur in superconductors. This rules out any generic explanation based on order-disorder (or Bragg glass to vortex glass) transition, and resolves the difficulty in interpreting the PE in thin amorphous films. Also, the simulation results cannot be explained within LO theory. The R_c in the absence of dislocations in 2D was shown to be $\sim 4-5a_0$ [53], which is much smaller than the length scale determining the behaviour of I_c . Further, the amorphous regime also exists for $b \lesssim 0.2$ and occurs due to single vortex pinning. If the amorphous state in the PE regime is attributed to the single vortex pinning, one expects similar dynamical behaviour in the PE regime and in low fields. Contrarily, the anomalous dynamics is observed only in the PE regime, thus indicating that one need to go beyond the pinning concept to describe the vortex state in the PE regime.

As discussed in Section 3.4, an alternate scenario based on jamming can be invoked to explain the increase in I_c with increasing n_d . One of the important feature of a jammed state is the athermal relaxation under applied stress. For example, logarithmic relaxation is observed as a function of the number of ‘‘taps’’ applied to a granular heap[59]. Evidence for similar behaviour exists in vortex system in the PE region. Henderson *et al.*[14] showed that the voltage response with bi-directional current grows with the number of pulses before saturating, which is an evidence for athermal behaviour. In an interesting recent experiment Ravikumar *et al.*[60] measured the magnetic relaxation in V_3Si in the PE region. The authors found that the magnetic moment M as a function of serial number of measurement n (rather than the real time) follows logarithmic behaviour. If the measurement n is assumed to be the number of ‘‘taps’’ applied to the system[61], the athermal relaxation observed is similar to that observed in Ref.[59], indicating a common underlying mechanism in the two systems. More experiments and simulations are necessary to probe the jamming scenario in the vortex system in the PE region.

V. CONCLUSIONS

The paper describes the results from detailed simulation of the magnetic field dependence of I_c for a superconductor at $T = 0$. The $I_c(B)$ shows a large increase near the upper critical field B_{c2} in agreement with the experimental observation of the peak effect phenomenon. There is no evidence of a phase transition in the peak effect region. Instead, a continuous transformation of a less disordered polycrystalline state into an amorphous state is observed implying that an ordered state is not necessary for the PE to occur. A jamming scenario is presented which could explain the PE and can account

for the anomalous dynamics in the peak effect region.

Acknowledgments

M.C. acknowledges useful discussions with A. K. Grover, E. Zeldov, S. Bhattacharya, and Ravikumar during various stages of the work, and thanks G. T. Zimanyi and R. T. Scalettar for critical comments during the part of the work. The simulation was performed at the Albuquerque High Performance Computing Center, University of New Mexico, during the authors' stay at the University of California, Davis.

[1] T. G. Berlincourt, R. R. Hake, and D. H. Leslie, Phys. Rev. Lett. **6**, 671 (1961). See also W. DeSorbo, Rev. Mod. Phys. **36**, 90 (1964).

[2] M. Isino, T. Kobayashi, N. Toyota, T. Fukase, and Y. Muto, Phys. Rev. B **38**, 4457 (1988).

[3] M. J. Higgins and S. Bhattacharya, Physica C **257**, 232 (1996) and references there in.

[4] G. D' Anna, M. V. Indenbom, M.-O. Andr, W. Benoit, and E. Walker, Europhys. Lett. **25**, 225 (1994); D. Pal, D. Dasgupta, B. K. Sarma, S. Bhattacharya, S. Ramakrishnan, and A. K. Grover, Phys. Rev. B **62**, 6699 (2000).

[5] K. Tenya, M. Ikeda, T. Tayama, H. Mitamura, H. Amitasu, T. Sakakibara, K. Maezawa, N. Kimura, R. Settai, and Y. Onuki, J. Phys. Soc. Jap. **64**, 1063 (1995).

[6] A. Ishiguro, A. Sawada, Y. Inada, J. Kimura, M. Suzuki, N. Sato, and T. Komatsubara, J. Phys. Soc. Jap. **64**, 378 (1995).

[7] T. Tamegai, K. Behnia, N. Okuda, S. Ooi, T. Shibauchi, Z. Mao, and Y. Maeno, Physica B **284**, 543 (2000).

[8] M. Pissas, S. Lee, A. Yamamoto, and S. Tajima, Phys. Rev. Lett. **89**, 097002 (2002).

[9] R. Wördenweber, P. H. Kes, and C. C. Tsuei, Phys. Rev. B, **33**, 3172 (1986) and references there in.

[10] S. S. Banerjee, S. Ramakrishnan, A. K. Grover, G. Ravikumar, P. K. Mishra, V. C. Sahni, C. V. Tomy, G. Balakrishnan, D. Mck. Paul, P. L. Gammel, D. J. Bishop, E. Bucher, M. J. Higgins, and S. Bhattacharya, Phys. Rev. B **62**, 11838 (2000).

[11] E. Y. Andrei, Z. L. Xiao, W. Henderson, Y. Paltiel, E. Zeldov, M. Higgins, S. Bhattacharya, P. Shuk, and M. Greenblatt, Condensed Matter Theories **16**, 241 (2001).

[12] J. A. Good and E. J. Kramer, Phil. Mag. **24**, 339 (1971).

[13] Z. L. Xiao, E. Y. Andrei, and M. J. Higgins, Phys. Rev. Lett. **83**, 1664 (1999).

[14] W. Henderson, E. Y. Andrei, and M. J. Higgins, Phys. Rev. Lett. **81**, 2352 (1998).

[15] S. O. Valenzuela and V. Bekeris, Phys. Rev. Lett. **84**, 4200 (2000); *ibid.* **86**, 504 (2001).

[16] S. B. Roy, P. Chaddah, and P. Chaudhary, Phys. Rev. B **62**, 9191 (2000).

[17] S. S. Banerjee, N. G. Patil, S. Ramakrishnan, A. K. Grover, S. Bhattacharya, G. Ravikumar, P. K. Mishra, T. V. Chandrasekhar Rao, V. C. Sahni, and M. J. Higgins, Appl. Phys. Lett. **74**, 126 (1999).

[18] A. B. Pippard, Phil Mag. **19**, 217 (1969).

[19] A. I. Larkin, and Yu. N. Ovchinnikov, J. Low. Temp. Phys. **34**, 409 (1979).

[20] P. H. Kes and C. C. Tsuei, Phys. Rev. B **28**, 5126 (1983); P. Koorevaar, J. Aarts, P. Berghuis, and P. H. Kes, Phys. Rev. B **42**, 1004 (1990).

[21] G. Sambandamurthy, K. Das Gupta, and N. Chandrasekhar, Phys. Rev. B **63**, 214519 (2001).

[22] P. L. Gammel, U. Yaron, A. P. Ramirez, D. J. Bishop, A. M. Chang, R. Ruel, L. N. Pfeiffer, E. Bucher, G. D'Anna, D. A. Huse, K. Mortensen, M. R. Eskildsen, and P. H. Kes, Phys. Rev. Lett. **80**, 833 (1998).

[23] X. Ling, C. Tang, S. Bhattacharya, and P. M. Chaikin, Europhys. Lett. **35**, 597 (1996).

[24] D. G. Grier, C. A. Murray, C. A. Bolle, P. L. Gammel, D. J. Bishop, D. B. Mitzi and A. Kapitulnik, Phys. Rev. Lett. **66**, 2270 (1991).

[25] E. M. Forgan, D. McK. Fault, H. A. Mook, P. A. Timmins, H. Keller, S. Sutton, and J. S. Abell, Nature **343**, 735 (1990).

[26] T. Giamarchi and P. Le Doussal, Phys. Rev. Lett. **72**, 1530 (1994); Phys. Rev. B **52**, 1242 (1995).

[27] T. Nattermann and S. Scheidl, Adv. Phys. **49**, 607 (2000).

[28] T. Giamarchi and P. Le Doussal, Phys. Rev. B **55**, 6577 (1995).

[29] Y. Paltiel, E. Zeldov, Y. Myasoedov, M. L. Rappaport, G. Jung, S. Bhattacharya, M. J. Higgins, Z. L. Xiao, E. Y. Andrei, P. L. Gammel, and D. J. Bishop, Phys. Rev. Lett. **85**, 3712 (2000).

[30] G. Ravikumar, V. C. Sahni, A. K. Grover, S. Ramakrishnan, P. L. Gammel, D. J. Bishop, E. Bucher, M. J. Higgins, and S. Bhattacharya, Phys. Rev. B **63**, 024505 (2001).

[31] M. Marchevsky, M. J. Higgins, and S. Bhattacharya, Nature **409**, 591 (2001).

[32] Y. Paltiel, E. Zeldov, Y. N. Myasoedov, H. Shtrikman, S. Bhattacharya, M. J. Higgins, Z. L. Xiao, E. Y. Andrei, P. L. Gammel, and D. J. Bishop, Nature **403**, 398 (2000).

[33] C. Zeng, P. L. Leath, and D. S. Fisher, Phys. Rev. Lett. **82**, 1935 (1999).

[34] Y. Fasano, M. Menghini, F. de la Cruz, Y. Paltiel, Y. Myasoedov, E. Zeldov, M. J. Higgins, and S. Bhattacharya, Phys. Rev. B **66**, 020512(R) (2002).

[35] R. Schleser, P. J. E. M. van der Linden, P. Wyder, and A. Gerber, Phys. Rev. B **67**, 134516 (2003).

- [36] Min-Chul Cha and H. A. Fertig, Phys. Rev. Lett. **80**, 3851 (1998).
- [37] C. Reichhardt, K. Moon, R. Scalettar, and G. T. Zimányi, Phys. Rev. Lett. **83**, 2282 (1999).
- [38] A. van Otterlo, R. T. Scalettar, and G. T. Zimányi, R. Olsson, A. Petrean, W. Kwok, and V. Vinokur, Phys. Rev. Lett. **84**, 2493 (2000).
- [39] C.J. Olson, C. Reichhardt, R.T. Scalettar, G.T. Zimányi, and N. Grønbech-Jensen, Physica C, **384**, 143 (2003).
- [40] J. R. Clem, J. Low. Temp. Phys. **18**, 427 (1975); Z. Hao and J. R. Clem, M. W. McElfresh, L. Civale, A. P. Malozemoff, and F. Holtzberg, Phys. Rev. B **43**, 2844 (1991).
- [41] E. H. Brandt, Rep. Prog. Phys. **58**, 1465 (1995).
- [42] G. W. Crabtree, D. O. Gunter, H. G. Kaper, A. E. Koshelev, G. K. Leaf, and V. M. Vinokur, Phys. Rev. B **61**, 1446 (2000).
- [43] M. Tinkham, *Introduction to Superconductivity*, McGraw Hill, New York (1975).
- [44] S. Ryu and D. Stroud, Phys. Rev. B **54**, 1320 (1996).
- [45] Mahesh Chandran, cond-mat/0103263.
- [46] The I_c can also be defined as the current at which the dynamic resistance $\frac{dV}{dI}$ first becomes 0 as I is reduced. The I_c from this definition does not differ more than 2σ from the criterion used, where σ is the step by which the current is changed in obtaining the $V(I)$ curve around I_c .
- [47] W. Henderson, E. Y. Andrei, M. J. Higgins and S. Bhattacharya, Phys. Rev. Lett. **77**, 2077 (1996).
- [48] H. J. Jensen, A. Brass, and A. J. Berlinsky, Phys. Rev. Lett. **60**, 1676 (1988); H. J. Jensen, A. Brass, A. Shi, and A. J. Berlinsky, Phys. Rev. B **41**, 6394 (1990).
- [49] C. J. Olson, C. Reichhardt, and F. Nori, Phys. Rev. Lett. **81**, 3757 (1998).
- [50] N. Grønbech-Jensen, A. R. Bishop, and D. Domínguez, Phys. Rev. Lett. **76**, 2985 (1996).
- [51] Mahesh Chandran, R. T. Scalettar, and G. T. Zimányi, Phys. Rev. B **67**, 052507 (2003).
- [52] S. Bhattacharya and M. J. Higgins, Phys. Rev. Lett. **70**, 2617 (1993).
- [53] Mahesh Chandran, R. T. Scalettar, and G. T. Zimányi, Phys. Rev. B **69**, 024526 (2004).
- [54] Similar amorphous regime exists for low fields ($b \rightarrow 0$), as discussed in Ref.[53].
- [55] A. M. Troyanovski, M. van Hecke, N. Saha, J. Aarts, and P. H. Kes, Phys. Rev. Lett. **89**, 147006 (2002).
- [56] C. S. O'Hern, L. E. Silbert, A. J. Liu, and S. R. Nagel, cond-mat/0304421.
- [57] M.-Carmen Miguel, A. Vespignani, M. Zaiser, and S. Zapperi, Phys. Rev. Lett. **89**, 165001 (2002); M.-Carmen Miguel, J. S. Andrade Jr., S. Zapperi, cond-mat/0304555 (unpublished).
- [58] G. D' Anna, and F. Nori, Phys. Rev. Lett. **85**, 4096 (2000).
- [59] J. B. Knight, C. G. Fandrich, C. N. Lau, H. M. Jaegar, and S. R. Nagel, Phys. Rev. E **51**, 3957 (1995).
- [60] G. Ravikumar, M. R. Singh, and H. Küpfer, cond-mat/0309494.
- [61] In Ref.[60], the magnetization M was measured in a SQUID magnetometer where the sample undergoes excursion in a small inhomogeneous field. This generates a driving current near the surface of the sample. The Lorentz force due to this additional current can be thought as providing the “tapping” force for the vortex system.